Design Exploration of the NACA Airfoil Family Using High-Fidelity CFD Analysis

Mihai-Vladut HOTHAZIE*[,1,2], Daniel-Eugeniu CRUNTEANU[2],
Mihai-Victor PRICOP[1,2], Ionut BUNESCU[1,2], Mara-Florina NEGOITA[1,2],
Mihaita-Gilbert STOICAN[1,2]

*Corresponding author
[1]INCAS – National Institute for Aerospace Research "Elie Carafoli",
B-dul Iuliu Maniu 220, 061126, Bucharest, Romania,
hothazie.mihai@incas.ro*, daniel.crunteanu@upb.ro, pricop.victor@incas.ro,
bunescu.ionut@incas.ro, negoita.mara@incas.ro, stoican.gilbert@incas.ro
[2]National University of Science and Technology POLITEHNICA Bucharest,
Str. Gheorghe Polizu 1-7, 011061, Bucharest, Romania

DOI: 10.13111/2066-8201.2025.17.2.4

Received: 06 May 2025/ Accepted: 29 May 2025/ Published: June 2025
Copyright © 2025. Published by INCAS. This is an "open access" article under the CC BY-NC-ND license (http://creativecommons.org/licenses/by-nc-nd/4.0/)

Abstract: *As the aviation industry continues to prioritize sustainability, enhancing aerodynamic efficiency remains a central goal in reducing environmental impact. This study employs a high-fidelity Computational Fluid Dynamics (CFD) approach to improve the accuracy and reliability of airfoil shape optimization. Although such methods come with higher computational demands, advancements in processing power have recently transformed CFD-based analysis into feasible technique for two-dimensional aerodynamic optimization processes. To identify optimal airfoil configurations, two evolutionary algorithms are utilized: the Genetic Algorithm (GA) and the Differential Evolution Algorithm (DE). For clarity and straightforward interpretation, the NACA 4-digit airfoil parametrization method is adopted, offering an intuitive way to associate shape parameters, such as camber, thickness, and camber position, to their physical meaning. Additionally, a parametric analysis of the design space is conducted to assess the influence of each parameter and the behavior of the overall objective function. The paper concludes with a comparative evaluation of the optimization strategies, providing insight into their effectiveness in high-fidelity aerodynamic shape optimization.*

Key Words: *CFD, optimization, parametric studies, Differential Evolution, NACA 4-digit*

1. INTRODUCTION

With the rapid evolution of aviation technologies, the pursuit of high-efficiency aerodynamic shapes has become a central focus in modern aircraft design. Enhancing aerodynamic efficiency leads to reduced fuel consumption, thereby improving operational performance and contributing to environmental sustainability. This growing emphasis has driven significant research into airfoil shape optimization using a variety of optimization strategies. However, the overall success of such efforts is closely tied to the fidelity of the aerodynamic models employed. Historically, optimization studies have favored low-fidelity models, such as linearized potential flow solvers, mainly due to their low computational cost. While such tools may provide good estimations of aerodynamics characteristics under attached flow conditions

[1], they fall short in capturing viscous effects with sufficient accuracy [2]. This limitation can result in optimized shapes that do not perform as expected under more detailed analysis. As a result of advancements in computational resources [3], previously impractical high-fidelity simulations are now feasible, allowing for more precise aerodynamic evaluations without prohibitive time costs. To enable efficient parametric and optimization studies, various airfoil shape parametrization methods have been developed, offering continuous design space exploration. The effectiveness of these methods, however, is strongly influenced by the number of parameters involved. A well-designed parametrization must balance flexibility and simplicity, ensuring the design space is sufficiently large without becoming computationally inefficient [4], [5] . Existing techniques range from advanced approaches such as Class-Shape Transformation [7], Hicks-Henne functions [7], and Bézier curve-based methods [8], to more traditional ones like PARSEC [9] and NACA families [10]. This study builds on previous work [11] by using the NACA 4-digit parametrization, chosen for its simplicity, ease of interpretation, and computational efficiency. The primary goal of this research is to establish an automated optimization framework that integrates a high-fidelity CFD solver with an in-house stochastic optimization algorithm. ANSYS Fluent was employed for both the optimization procedure and the accompanying parametric analysis. The aerodynamic characteristics of the resulting configurations was evaluated and compared, with findings discussed in detail from both the optimization procedure as well as the parametric study.

2. METHODOLOGY

A. Airfoil Parametrization

The methodology employed in this study is divided into two main parts. The first part involves the automation of the CFD solver used to evaluate the objective function. The second part focuses on the optimization procedure, which is carried out using the Differential Evolution algorithm, followed by a parametric exploration of the design space. To facilitate better visualization and interpretation of the results, the NACA 4 digit parametrization method was selected. In this approach, the airfoil geometry is defined by three key parameters: M, the maximum camber as a percentage of the chord; P, the position of maximum camber in tenths of the chord; and T, the maximum thickness as a percentage of the chord, as illustrated in Figure 1.

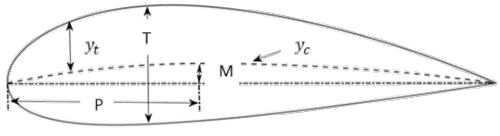

Figure 1. Representation of the NACA 4-digit airfoil parameters.

The airfoil geometry is constructed by adding a thickness distribution function y_T perpendicular to the camber line described by the function y_c. The mathematical expression for the camber line is defined as:

$$y_c = \begin{cases} \frac{M}{P^2}(2Px - x^2), & 0 \le x < P \\ \frac{M}{(1-P)^2}(1 - 2P + 2Px - x^2), & P \le x \le 1 \end{cases} \quad (1)$$

Similarly, the thickness distribution function, y_T, is given by the following equation:

$$y_T = \frac{T}{0.2}(a_0 x^{0.5} + a_1 x + a_2 x^2 + a_3 x^3 + a_4 x^4)$$
$$a_0 = 0.2969, \quad a_1 = -0.126, \quad a_2 = -0.3516, \quad a_3 = 0.2843, \quad a_5 = -0.1036 \tag{2}$$

Using (1) and (2), the coordinates of the upper and lower surfaces of the airfoil are obtained by adding or subtracting the thickness distribution perpendicular to the camber line, as defined by the following expressions:

$$\begin{aligned} Upper\ Surface \quad & x_u = x_c - y_t sin\theta \quad y_u = y_c + y_t cos\theta \\ Lower\ Surface \quad & x_l = x_c + y_t sin\theta \quad y_l = y_c - y_t cos\theta \\ & \theta = \text{atan}\left(\frac{dy_c}{dx}\right) \end{aligned} \tag{3}$$

To more accurately capture the airfoil's curvature, a cosine spacing distribution is employed with uniform increments of the angle β:

$$x = \frac{1 - cos\beta}{2}, \quad 0 \le \beta \le \pi \tag{4}$$

B. Aerodynamic Evaluation

The aerodynamic characteristics of the airfoil were evaluated through numerical simulations based on the Reynolds-Averaged Navier–Stokes equations, where the conservation of mass and momentum are expressed as follows:

$$\frac{\partial}{\partial x_i}(\rho u_i) = 0$$
$$\frac{\partial(\rho u_i u_j)}{\partial x_j} = \frac{\partial p}{\partial x_i} + \frac{\partial}{\partial x_i}\left(\mu\left(\frac{\partial u_i}{\partial x_j} + \frac{\partial u_j}{\partial x_i} - \frac{2}{3}\delta_{ij}\frac{\partial u_j}{\partial x_i}\right)\right) + \frac{\partial}{\partial x_j}\left(-\rho\overline{\acute{u}_i\acute{u}_j}\right) + \rho f_b \tag{5}$$

where density ρ, pressure p, dynamic viscosity μ, velocity components u_i, u_j and the Reynolds stress $\frac{\partial}{\partial x_j}\left(-\rho\overline{\acute{u}_i\acute{u}_j}\right)$ represent the unknown terms. To nonlinear term denoted by the Reynolds stress accounts for anisotropic turbulence, where $\acute{u}_i$, $\acute{u}_j$ represent the fluctuating components of the corresponding velocities. The shear stress transport model represents a two equations eddy-viscosity hybrid model which combines the Wilcox $k-\omega$ and $k-\epsilon$ models using a blending function F_1 which ensures that the appropriate model is used based on the wall distance. The two equations related to the turbulent kinetic energy k and turbulent dissipation rate ω in the SST turbulence model are given by the following equations:

$$\frac{\partial}{\partial t}(\rho k) + \frac{\partial}{\partial x_i}(u_i \rho k) = \frac{\partial}{\partial x_i}\left(\frac{\mu_k \partial}{\partial x_i} k\right) + \widetilde{P_k} - \beta^* \rho \omega k$$
$$\frac{\partial}{\partial t}(\rho \omega) + \frac{\partial}{\partial x_i}(u_i \rho \omega) = \frac{\partial}{\partial x_i}\left(\mu_\omega \frac{\partial}{\partial x_i}\omega\right) + \alpha \rho S^2 - \beta \rho \omega^2 + \tag{6}$$
$$2\rho(1 - F_1)\sigma_{\omega^2}\frac{1}{\omega}\frac{\partial}{\partial x_i}k\frac{\partial}{\partial x_i}\omega$$

The blending function F_1 is as follows:

$$F_1 = tanh\left\{\left\{min\left[max\left(\frac{\sqrt{k}}{\beta^*\omega y}, \frac{500v_\infty}{y^2\omega}\right), \frac{4\rho\sigma_{\omega^2}k}{CD}\right]\right\}^4\right\} \tag{7}$$

where $C_{D_{k\omega}}$ represents the cross-diffusion term, μ_k and μ_ω represents the effective velocities and are expressed in terms of the turbulent viscosity μ_t and the blending factor F_2 as follows:

$$\begin{aligned} \mu_k &= \mu + \sigma_k\mu_t \\ \mu_\omega &= \mu + \sigma_\omega\mu_t \\ \mu_t &= \frac{a_1 k}{\max(a_1\omega, SF_2)} \\ F_2 &= \left[\left[\max\left(2\frac{\sqrt{k}}{\beta^*\omega y}, \frac{500v}{y^2\omega}\right)\right]^2\right] \end{aligned} \tag{8}$$

The operating conditions are: $Re = 6 \times 10^6$, $V_\infty = 51\, m/s$, $\rho = 1.77\, kg/m^3$, $\mu = 1.645 \times 10^{-5}\, kg \cdot m^{-1} \cdot s^{-1}$, $\alpha = 2°$, and the flow is assumed to be steady, incompressible, and fully turbulent. A *C*-type computational domain was employed, as in Figure 2 , where R represents the design parameter of the domain, with R = 100 m used in this study.

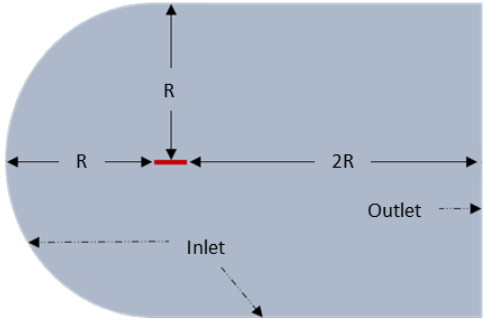

Figure 2. Representation of the C-type computational domain

The grid was adapted with near wall mesh cell height corresponding to $y^+ = 1$, with a global growth ratio of 1.1 as can be seen in Figure 3. The boundary layer is generated with an imposed first cell height of 1.4×10^{-5} and a number of 40 layers with a growth ratio of 1.1. The grid is generated using Ansys Meshing and a no-slip condition is applied on the surface of the airfoil.

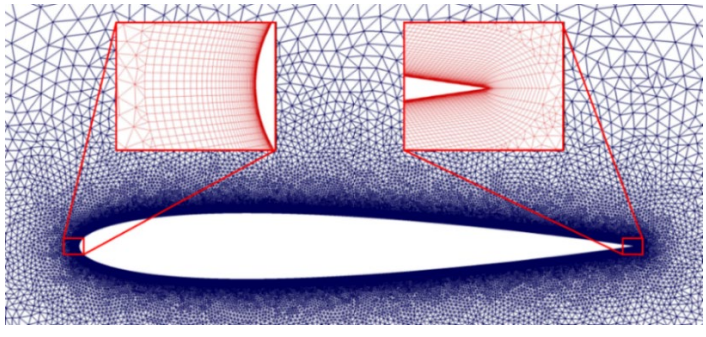

Figure 3. Computational grid layout with detailed views of the near-wall mesh refinement.

The automated process developed to evaluate the objective function using high-fidelity CFD involves several successive steps. First, the airfoil coordinates are generated using a MATLAB script. Then, ANSYS Workbench is called via a Windows batch file, and the Design Modeler module is accessed through a Python script. Within Design Modeler, a JScript routine is used to generate the computational domain by importing the airfoil geometry. Next, the geometry is passed to ANSYS Meshing, where another JScript script generates the computational grid. The resulting mesh is then exported in Fluent-compatible format. Finally, the mesh is imported into ANSYS Fluent, and a journal file is executed to perform the aerodynamic analysis. This script automates the simulation process and extracts the aerodynamic characteristics of the analyzed airfoil. A schematic overview of the automation workflow is presented in Figure 4.

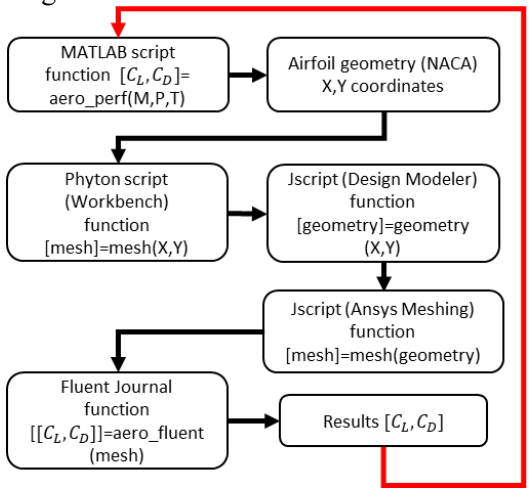

Figure 4. Logical scheme of the automation process for evaluating the objective function using high-fidelity CFD.

C. Optimization Technique

When addressing highly complex optimization problems, stochastic methods are often preferred due to their ability to escape local minima and explore a larger solution space, thereby increasing the likelihood of identifying the global solutions [12]. For this reason, a stochastic algorithm was chosen to implement using an in-house code due to its ability to properly explore a large design space. A general constrained optimization problem can be formulated as presented in equation (9):

$$\begin{gathered} \min f(x) \ \ subjected\ to: \\ g_k(x) \leq 0, k = \overline{1,k} \\ h_l(x) = 0, l = \overline{1,L}, \mathrm{L} < \mathrm{n} \\ l^k \leq x^j \leq u^j, j = \overline{1,n} \end{gathered} \tag{9}$$

where $g_k(x)$ is the inequality vector constraint, $h_k(x)$ is the equality vector constraint l^k, u^k represent the lower and upper boundaries of the search domain.

A free parameter scheme was chosen where a modified fitness function is introduced which takes into account the original fitness function, $f(x_{i,g})$, a constrained violation function, $G(x_{i,g})$, and an additional penalty term $\theta_g(x_{i,g})$ that guarantees that all infeasible points will have worse fitness function values than any feasible ones.

Another benefit of the penalty term in the optimization process is that it directs the optimization process to a feasible region. The penalty term is expressed as follows:

$$\theta_g(x_{i,g}) = \begin{cases} 0 & if \quad x_{i,g} \in \Omega \\ -f(x_{i,g}) & if \quad s_g \in \Omega = \emptyset \\ -f(x_{i,g}) + \max\limits_{y \in S_g \cap \Omega} f(x_{i,g}) & if \quad s_g \in \Omega = \emptyset \; x_{i,g} \notin \Omega \end{cases} \tag{10}$$

Having the optimization parameters defined in the parametrization method used to generate a continuous range of airfoil geometries, the mathematical formulation of the objective function for aerodynamic optimization, where the goal is to maximize the lift-to-drag ratio, can be expressed as follows:

$$minimize\ f_{obj}(x_{i,g}) = \frac{C_D}{C_L}, subjected\ to\ \ lb \le x_{i,g} \le up \tag{11}$$

The main advantage over other algorithms from the same category is the low number of adjusting parameters needed to be tailored for the specific problem: the population size, NP, the scalability factor, F, and the crossover probability, CR. In our case, a free parameter scheme was used where the optimization is executed on a modified fitness function $\hat{f}(x_{i,g})$ which represents the summation between the original fitness function $f(x_{i,g})$, the constraint violation function $G(x_{i,g})$, and an additional penalty term $\theta_g(x_{i,g})$. Using a population of candidate solutions, the next generation is created by applying mutation defined by the following expression:

$$\hat{X}_i^{g+1} = X_{r_1}^g + F(X_{r_2}^g - X_{r_1}^g) \tag{12}$$

After that, a crossover operation followed by an elitism operator is applied to generate the next population and steer the individuals through the design space to the optimum solution. The process is repeated until the stopping criterion is met. In the Differential Evolution algorithm, three key parameters govern the optimization process: the mutation factor (F), which controls the scale of the mutation step and contributes to the exploration of the search space, the Crossover Rate (CR), which maintains population diversity and the Population Size (NP), which influences the algorithm's ability to thoroughly explore the design domain.

The presented airfoil shape optimization procedure, using an in-house differential evolution code, was also compared with another evolutionary algorithm, the Genetic Algorithm from MATLAB's Global Optimization Toolbox to ensure the best possible outcomes [13]. A general logical scheme for both the Genetic Algorithm and Differential Evolution is presented in Figure 5.

Within the optimization loop, the most computationally expensive step is the evaluation of the objective function. However, recent advancements in computational resources, including multicore workstations, have significantly reduced the time required for aerodynamic performance evaluations using high-fidelity CFD. This improvement enables a more effective optimization process. The automation procedure described earlier is integrated within the optimization loop to perform aerodynamic performance predictions, serving as the objective function evaluation.

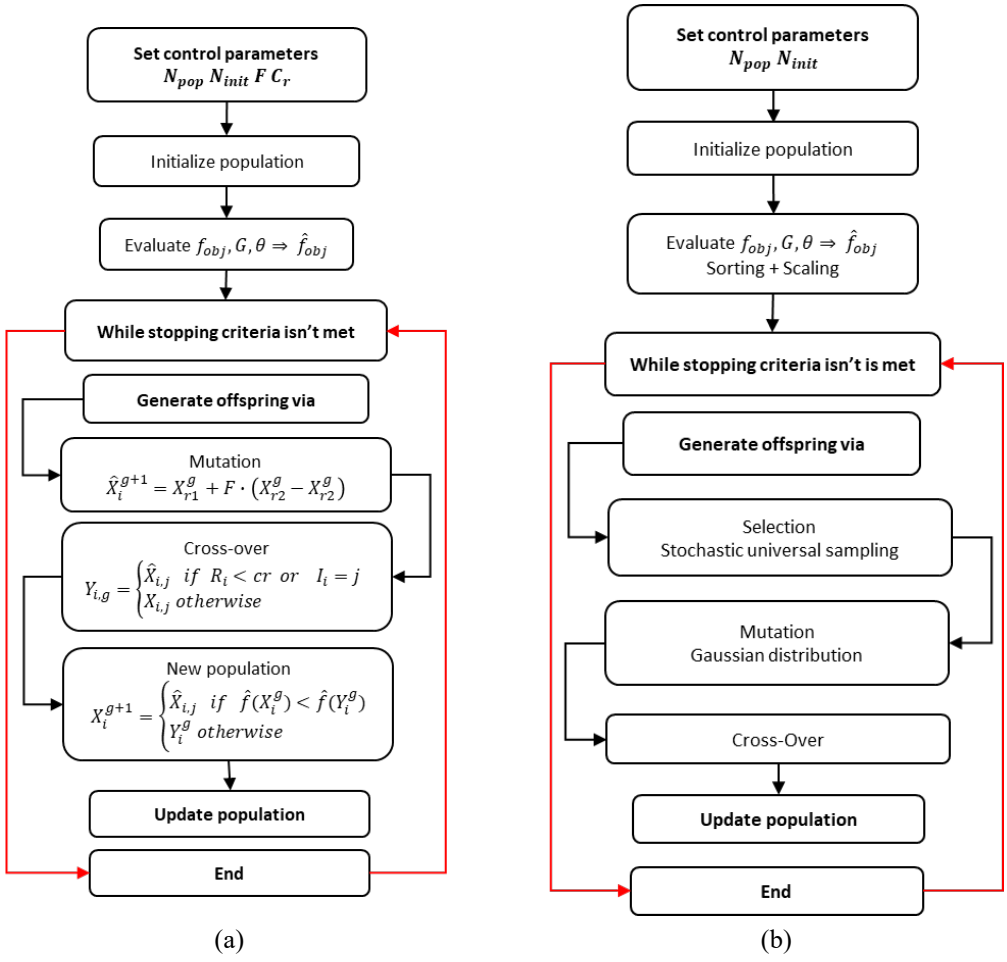

Figure 5. General logical scheme for Differential Evolution in-house algorithm (a) and Genetic Algorithm (b).

3. RESULTS

After performing the aerodynamic shape optimization to maximize the lift-to-drag ratio, the results are presented as follows. First, a convergence study examining the impact of population size on each optimization algorithm is shown to ensure result accuracy.

Then, a comparison between the algorithms is made by analyzing the convergence of each parameter at the maximum population size. Finally, a parametric study of the design space is performed to validate the optimal values and to visualize the behavior of the objective function in the design space.

As shown in Figure 6, when using the high-fidelity solver, the Genetic Algorithm demonstrates consistent convergence across varying population sizes, except for the smallest population where some variation is observed. For the largest population size, the algorithm reaches the optimum value by the 8th generation. These observations suggest that the objective function may not be highly complex.

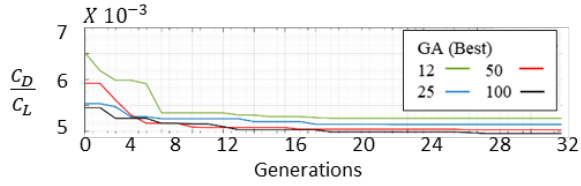

(a)

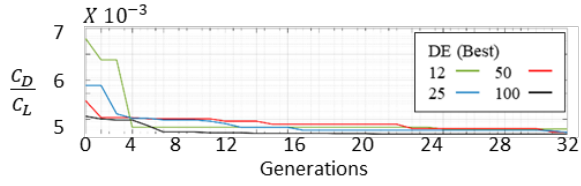

(b)

Figure 6. Convergence study with respect to population size for each optimization algorithm: (a) Genetic Algorithm, (b) Differential Evolution,

The convergence behavior of both algorithms for each optimization variable is illustrated in Figure 7. The results indicate that the maximum camber (M) and the maximum thickness (T) converged to identical values for both the Differential Evolution and Genetic Algorithm. However, the position of the maximum camber (P) differed between the two approaches.

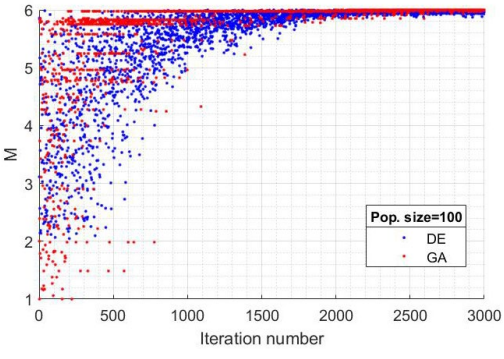

(a)

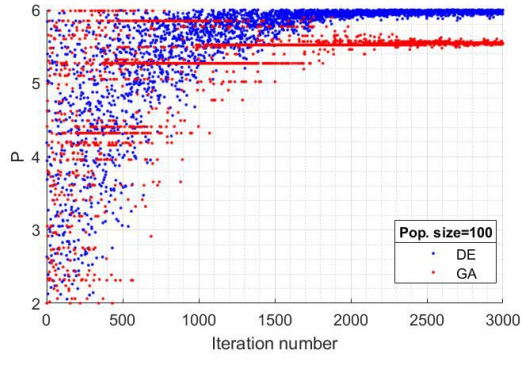

(b)

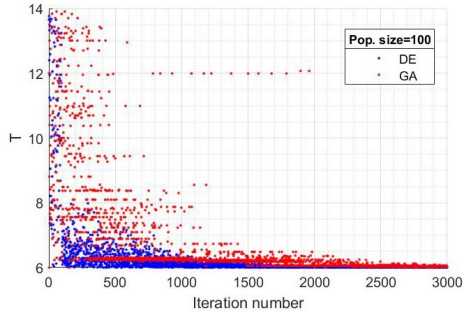

(c)

Figure 7. Convergence plots of each optimization variable: (a) maximum camber (M), (b) position of maximum camber (P), and (c) maximum thickness (T), for both optimization algorithms.

A convergence plot of the aerodynamic performance versus iteration number is presented in Figure 8. The results indicate that both the Genetic Algorithm and Differential Evolution

converged within the same basin of attraction, with slight differences in the position of the maximum value obtained. This suggests that the design space may contain multiple basins of convergence or local optima. Despite the small difference in predicted performance, the error between the two algorithms is negligible, indicating that both successfully identified the optimal region. Moreover, due to the elitism strategy used in DE, the algorithm does not explicitly preserve the best candidate from one generation to the next, allowing the solution to evolve more naturally. While this may lead to slower convergence, it improves the algorithm's ability to explore complex design spaces thoroughly.

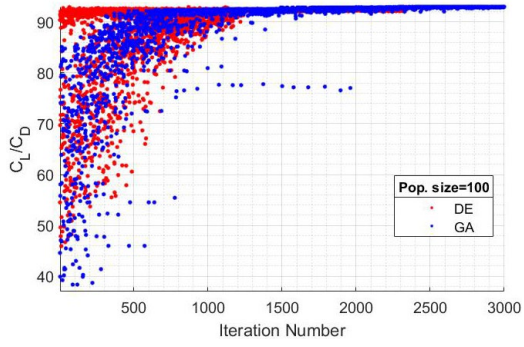

Figure 8. Vortex generators positions for every case

To further validate the results, Figure 9 presents a three-dimensional parametric study. The maximum thickness T is plotted on the X-axis, the maximum camber M on the Y-axis, and the aerodynamic performance on the Z-axis. The color-coded planes represent varying values of the position of maximum camber (P), ranging from 20% to 60% of the chord length.

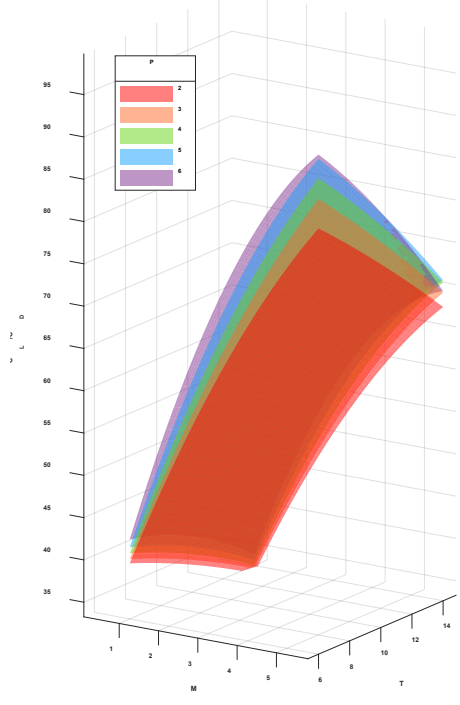

(a)

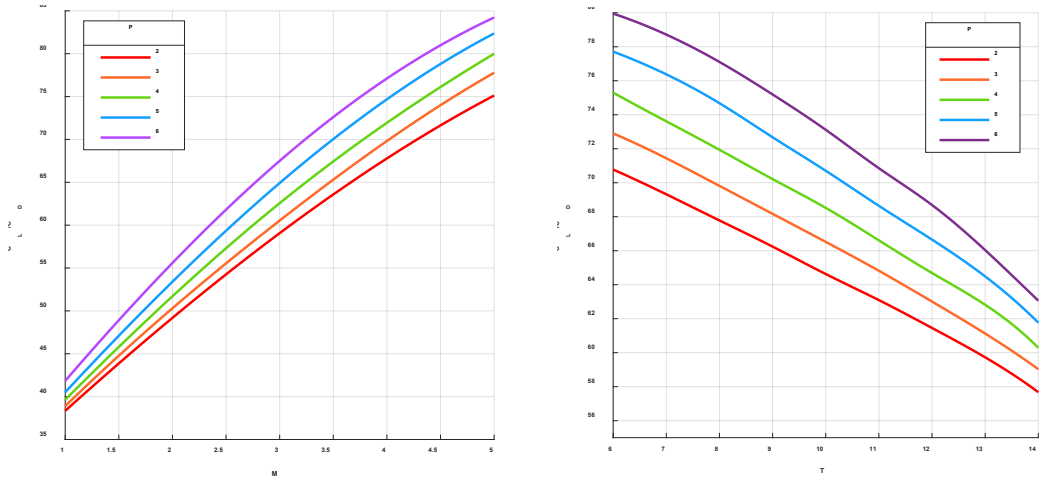

(b) **(c)**

Figure 9. 3D parametric study of lift-to-drag ratio: (a) versus thickness (T), camber (M), and camber position (P); (b) versus M and P at T = 8; (c) versus T and P at M = 4.

The surfaces obtained using the high-fidelity solver exhibit a quasi-parallel and well-structured behavior, indicating a smooth and predictable objective function landscape. This characteristic explains why, during the optimization process with the high-fidelity solver, the Genetic Algorithm (GA) was able to consistently reach the optimum within the same maximum number of generations across all population sizes, except for the smallest one. In contrast, the Differential Evolution (DE) algorithm demonstrated a different behavior: it showed improved performance with smaller population sizes when dealing with complex problem spaces, while it required larger populations to converge effectively in simpler scenarios. These observations suggest that DE may be more suitable for complex optimization problems due to its efficient exploration capabilities and lower computational demands, whereas GA may be more effective for simpler problems where rapid convergence is desirable. In addition, the parametric study highlights the influence of each design parameter on aerodynamic performance. Increasing the airfoil thickness generally results in a decrease in the lift-to-drag ratio, likely due to increased drag. In contrast, increasing the maximum camber improves the lift-to-drag ratio, indicating that greater curvature enhances lift generation. Moreover, shifting the position of the maximum camber toward the trailing edge also tends to increase the lift-to-drag ratio, suggesting aerodynamic benefits for this type of airfoils.

5. CONCLUSIONS

The importance of using a high-fidelity solver in airfoil shape optimization is emphasized through both optimization and parametric studies. An in-house optimization framework based on the Differential Evolution algorithm was developed to carry out the optimization process. To ensure the reliability of the results, a second well-established optimization method, the Genetic Algorithm from MATLAB's Global Optimization Toolbox, was also employed for comparison. The second part of this work focuses on parametric analyses that provide insight into the behavior of the objective function and the influence of design variables. Although the use of a high-fidelity solver involves increased computational effort, the resulting parametric surfaces allow for a clearer understanding of the design space and the identification of optimal configurations. The NACA 4-digit airfoil parametrization was selected for demonstration

purposes due to its simplicity and interpretability. However, the validated methodology presented in this study can be extended to more advanced parametrization techniques such as Class-Shape Transformation or Hicks-Henne bump functions. Additionally, the fully automated process developed for high-fidelity aerodynamic performance evaluation using Fluent offers a robust foundation for future research, including the optimization of high-lift devices or airfoils operating in transonic regimes. To further improve efficiency, future work could explore hybrid optimization strategies that combine stochastic and deterministic methods to accelerate convergence while maintaining solution quality.

REFERENCES

[1] S. A. Glegg and W. J. Devenport, Panel methods for airfoils in turbulent flow, *Journal of Sound and Vibration,* vol. **329**, no. 18, pp. 3709-3720, 2010.

[2] J. Morgadoa, R. Vizinhob, M. Silvestrea and J. Páscoab, XFOIL vsCFD performance predictions for high lift low Reynoldsnumber airfoils, *Aerospace Science and Technology,* no. **52**, pp. 207-214, 2016.

[3] E. J. Nielsen and B. Diskin, High-performance aerodynamic computations for aerospace applications, *Parallel Computing,* 2014.

[4] B. Zheng, A. Moni, W. Yao and M. Xu, Manifold Learning for Aerodynamic Shape Design Optimization, *MDPI Aerospace,* vol. **258**, no. 3, 2025.

[5] J. V. B. Santos, V. G. P. Siston, G. A. P. Campos and J. L. Z. Zotin, Analysis of Parametrization Methods for Aerodynamic Profiles, *Associacao Brasileira de Engenharia e Ciencias Mecanicas,* 2020.

[6] B. M. Kulfan, Universal parametric geometry representation method, *Journal of Aircraft,* vol. **45**, no. 1, pp. 142-158, 2008.

[7] Y. Dai, F. Peng, C. Yang, X. Liu, M. Yuan and B. He, Optimal Design of FSAE Airfoils Based on Hicks-Henne Function, in *China SAE Congress 2023: Selected Papers. SAE-China 2023 Lecture Notes in Electrical Engineering,* vol **1151**, Springer, Singapore, 2024.

[8] T. Melin, *Parametric Airfoil Catalog, An Aerodynamic and Geometric Comparison Between Parametrized and Point Cloud Airfoils*, Linkoping, Sweden: Fluid and Mechatronic Systems, 2013.

[9] H. Sobieczky, Parametric Airfoils and Wings, *Notes on Numerical Fluids,* vol. **68**, pp. 71-88, 1998.

[10] C. Ladson and C. W. Brooks, *Development of a Computer Program to Obtain Coordinates for NACA 4-Digit, 4-Digit Modified and 16-Series Airfoil*, National Aeronautics and Space Administration, Washington D.C., 1975.

[11] M.-V. Hothazie, M.-V. Pricop and I. Bunescu, Low-speed airfoil optimization using CFD and low fidelity solvers, in *AIAA SCITECH 2023 Forum*, National Harbor, 2023.

[12] L. Liberti and S. Kucherenko, A comparison of deterministic and probabilistic optimization algorithms for nonsmooth simulation-based optimization, *Building and Environment,* vol. **39**, no. 8, pp. 989-999, 2004.

[13] * * * I. The MathWorks, MATLAB (R2020a), 2020. [Online]. Available: https://www.mathworks.com/help/gads/ga.html.